Bacterial adhesion and inactivation on Ag decorated TiO-nanotubes under visible light Effect of the nanotubes geometry on the photocatalytic activity

Ahmed El Hajjaji, M Elabidi, K Trabelsi, a A Assadi, B Bessais, S Rtimi

1

Bacterial adhesion and inactivation on Ag decorated TiO₂-nanotubes under visible light:

Effect of the nanotubes geometry on the photocatalytic activity.

A. Hajjaji [1], M. Elabidi [1], K. Trabelsi [1], A.A. Assadi [2], B. Bessais [1]** and S. Rtimi [3]*

[1] Laboratoire de Photovoltaïque, Centre de Recherches et des Technologies de l'Energie, Technopole de Borj-Cédria, BP 95, 2050 Hammam-Lif, Tunisia
[2] Ecole Nationale Supérieure de Chimie de Rennes, CNRS, ISCR (Institut des Sciences Chimiques de Rennes) – UMR 6226, F-35000 Rennes, France
[3] Ecole Polytechnique Fédérale de Lausanne (EPFL), EPFL-STI-IMX-LTP, Station 12, CH-1015, Lausanne, Switzerland
* Corresponding authors: S. Rtimi, sami.rtimi@epfl.ch, Tel: +41 21 693 6803

B. Bessais, brahim.bessais@crten.rnrt.tn, Tel: +216 79 325 215
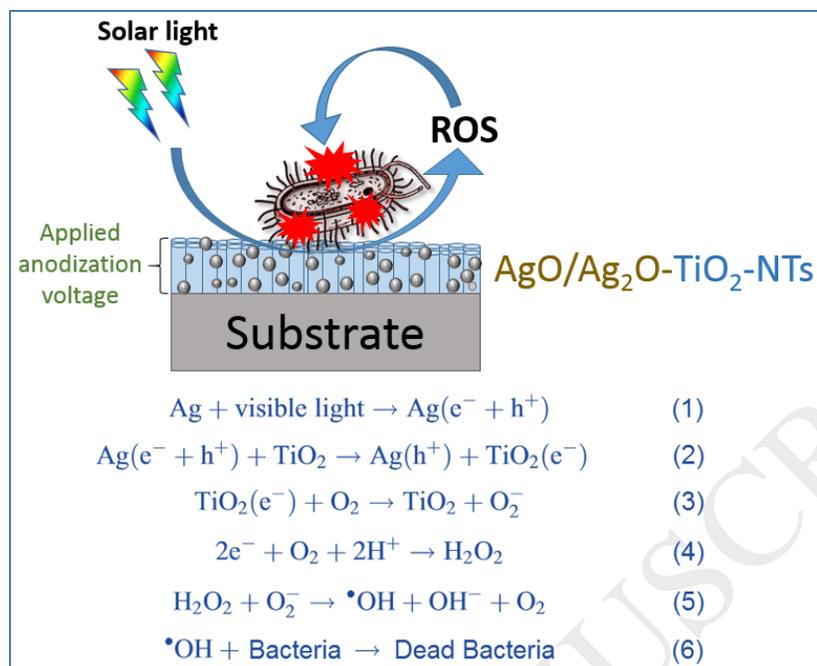
Statistical Summary:

Abstract: 292 words

Main manuscript words: 5414 (not including figures captions)

Number of Figures: 7

Number of Tables: 1

Graphical abstract:

Bacterial inactivation is seen to be related to the nanotubes anodization potential and the silver-ions decoration.

1

$$Ag + \text{visible light} \rightarrow Ag(e^- + h^+) \qquad (1)$$

$$Ag(e^- + h^+) + TiO_2 \rightarrow Ag(h^+) + TiO_2(e^-) \qquad (2)$$

$$TiO_2(e^-) + O_2 \rightarrow TiO_2 + O_2^- \qquad (3)$$

$$2e^- + O_2 + 2H^+ \rightarrow H_2O_2 \qquad (4)$$

$$H_2O_2 + O_2^- \rightarrow {}^\bullet OH + OH^- + O_2 \qquad (5)$$

$${}^\bullet OH + \text{Bacteria} \rightarrow \text{Dead Bacteria} \qquad (6)$$

Highlights :

- TiO$_2$ nanotubes decorated by silver nanoparticles were prepared
- Ag nanoparticles decoration was carried out using the photo-reduction process
- SEM and TEM imaging were used to see the microstructure of the nanotubes
- The effect of the NTs geometry on the bacterial inactivation was investigated

Abstract:

This study investigates the effect of the diameter of TiO$_2$ nanotubes and silver decorated nanotubes on optical properties and photocatalytic inactivation of *Escherichia coli* under visible light. The TiO$_2$ nanotubes (TiO$_2$-NTs) were prepared using the electrochemical method varying the anodization potential starting from 20V until 70V. The Ag nanoparticles were carried out using the photoreduction process under the same experimental conditions. The diameter size was determined using the scanning electronic microscopy (SEM). TiO$_2$-NTs diameter reached ~100 nm at 70V. Transmission electronic microscopy (TEM) imaging confirmed the TiO$_2$-NTs surface decoration by silver nanoparticles. The Ag-NPs average size was found to be equal to 8 nm. The X-Ray

diffraction (XRD) analysis confirm that all TiO_2-NTs crystallize in the anatase phases regardless the used anodization potential. The decrease of the photoluminescence (PL) intensity of Ag NPs decorated TiO_2-NTs indicates the decrease of the specific area when the nanotubes diameter increases. The UV-Vis absorbance show that the absorption edges was bleu shifted with the increasing of nanotubes diameter, which can be explained by the increase of the crystallites average size. The bacterial adhesion and inactivation tests were carried in the dark and under light. Bacteria were seen to adhere on TiO_2-NTs in the dark; however, under light the bacteria were killed before they establish a strong contact with the TiO_2-NTs and Ag/TiO_2-NTs surfaces. Bacterial inactivation kinetics were faster when the anodizing potential of the NTs-preparation increases. A total bacterial inactivation was obtained on ~100 nm nanotubes diameter within 90 min. This result was attributed to the enhancement of the TNTs crystallinity leading to reduced surface defects. Redox catalysis was seen to occur under light on the TiO_2-NTs and Ag/TiO_2-NTs. the photo-induced antibacterial activity on the AgO/Ag_2O decorated TiO_2-NTs was attributed to the interfacial charge transfer mechanism (IFCT).

Keywords: Ag decorated Titanium nanotubes, AgO/Ag_2O, Nanotubes geometry, Crystallinity, Bacterial adhesion, Bacterial inactivation.

1. INTRODUCTION

Escherichia coli (*E. coli*) is hazardous bacteria that can cause distinct diarrhea syndrome. it was recognized as pathogen because it can cause urinary tract infection, hemolytic uremic syndrome and thrombotic thrombocytopenic purpura in human [1]. Thus, it is necessary to develop an effective material for the inactivation of *E. coli*.

Currently, the inactivation of bacteria is mainly through chemical products based on chloride as strong oxidant. Unfortunately, a big majority of these poducts produce carcinogenic disinfection by-products (DBPs) like trihalomethanes and haloacetic acids [2]. Oher products are based on bactericidal nanoparticles (mainly silver). These later products are showing limitations towards some germs. In addition, some pathogens can develop resistance to silver nanoparticles as recently reported [3]. World Health Organization (WHO) launched an alert towards the excessive use of antibiotics and their derivatives [4]. Antibiotics are today showed to become ineffective against many pathogens that are able to develop resistance; hence, many germs became multidrug resistant. Thus, it is necessity today to develop alternative ways to disinfect surfaces in hospital facilities since healthcare acquired infections are increasingly threatening our lives [5-7].

Photocatalytic bacterial inactivation is found to be a promising alternative due to several advantages. The sustainable use of the photocatalytic material is one of the most unique properties of this method while conventional chemical root consumes disinfectants [8]. also this new method does not produce any toxic or carcinogenic product (DBPs). Additionally, Titanium dioxide (TiO_2) is attracting great attention during the last decades because of its chemical stability, non-toxicity, high oxidative power and low fabrication cost [5]. Titanium based photocatalysts have been used to inactivate bacteria (in the dark or under light irradiation) [9-10], virus [11] and even cancer cells/tumor [3-6]. However, the wide band gap energy (3.2 eV) and the high recombination rate of the photo-generated charges in TiO_2 reduces its photocatalytic performance. To overcome this limitation, many strategies can be adopted like modifying TiO_2 with anionic or cationic doping [12, 13], narrow-band semi-conductors coupling [14] or metallic nanoparticles decoration [15]. Although, it has been reported since years that anatase and rutile crystalline phases of TiO_2 are more active than brookite form [16]. With respect to the photocatalytic activity of the polymorphs, although it is somewhat controversial, the anatase phase is generally regarded as being more active than rutile [17,18]. An emerging field of interest in photocatalysis is the development of TiO_2 nanotubes (TiO_2-NTs) and their coupling with cations, metal-oxides and additional composites leading to a higher nanocomposite sensitization in the visible range [19-21]. Titanium anodization is a simple preparation leading to controllable nanotubes formation, chemical resistivity, high surface area (2-3 orders of magnitude higher than a flat surface) and therefore high loading capability. The large surface to volume ration of TiO_2-NTs is related to the large internal and external surfaces along with the surface in their vertex and the interstitial surface.

In this study, TiO_2-NTs were prepared by anodic oxidation. After optimization of the TiO_2-NTs antibacterial activity and geometry, the most active NTs were decorated with different amounts of silver nanoparticles (Ag NPs) using the photo-reduction method. We focus on the effect of NTs geometry before and after the Ag-decoration and its influence on the charge separation and transport. Furthermore, this decoration affected the optical properties and photocatalytic performance against *E. coli* under low intensity solar simulated light. We also show that varying the anodization potential during the nanotubes growth influences their geometry and reactivity under visible light.

2. EXPERIMENTAL

2.1. Preparation of Ag-NPs/TiO$_2$-NTs photo-electrodes

The anodization was performed under continuous stirring during 2 h at room temperature and at different potential starting from 20 V to 70 V. The electrolyte consisted of a mixture of 2 vol.% of water and ethylene glycol and 0.07 M of NH$_4$F. The as-prepared TiO$_2$-NTs were rinsed with water, air dried, and then annealed for 3 hours at 400°C (5°C/min). Subsequently, the prepared TiO$_2$-NTs were decorated with Ag-NPs using the photo-reduction method. To this end, the TiO$_2$-NTs were first immersed in a 0.1 M solution of AgNO$_3$ for 24 hours, then rinsed with water and immersed again in methanol under UV radiation (254 nm) for 10 minutes. Finally, the Ag-NPs/TiO$_2$-NTs samples were rinsed with water and dried in a vacuum oven for 1 h at 80°C.

2.2. Evaluation of the adhesion and inactivation of *E. coli* on Ag-NPs/TiO$_2$-NTs under light and dark conditions

The antibacterial activity of the Ag-NPs/TiO$_2$-NTs was performed taking *Escherichia coli* (*E. coli* K12 ATCC 23716; from the Deutsche Sammlung von Mikroorganismen und Zellkulturen GmbH (DSMZ), Braunschweig, Germany) as a probe. The samples were sterilized by autoclaving at 121°C for 2 h. The 100 μL culture aliquots with an initial concentration of ~4 10^6 Colony-forming unit per milliliter (CFU mL^{-1}) in NaCl/KCl (pH 7) were placed on the samples. The 100 μL of the *E. coli* inoculum was contacted with the Ag-NPs/TiO$_2$-NTs uniform surface. The exposition was done at 23°C (+/-2°). The samples were then placed on Petri dishes provided with a lid to prevent evaporation. After each determination, the surface was transferred into a sterile 2 mL Eppendorf tube containing 900 μL autoclaved NaCl/KCl saline solution. This solution was subsequently mixed thoroughly using a Vortex for 2 min. Serial dilutions were made in NaCl/KCl solution. A 100 μL sample of each dilution was pipetted onto a nutrient agar plate and then spread over the surface of the plate using standard plating method. Agar plates were incubated lid down, at 37 °C for 24h before colonies were counted. Three independent assays were done for each sample.

The statistical analysis of the results were performed for the CFU values calculating the standard deviation values. The average values were compared by one-way analysis of variance and with the value of statistical significance. The one-way analysis of variance (one-way ANOVA) was used to compare the mean of the samples using the Fisher distribution. The response variable was approximated for the sample data obtained from the photocatalytic inactivation of test samples presenting the same distribution within the same sample (prepared at fixed anodization voltage).

To verify that no attached/adsorbed bacteria remained on the surface, samples were incubated for 24 hours at 37°C on agar. No bacterial re-growth was observed.

The samples were irradiated in the cavity of an Atlas solar simulator (Atlas, GmbH, Hanau, Germany) with an overall power of 50 mW/cm^2 with light distribution wavelength distribution resembling solar irradiation emitting at wavelengths between 310 and 800 nm. The system contains an air-cooled Xenon lamp provided with filter to cut off wavelengths below 310 nm and above 800 nm. Samples were irradiated into covered glass petri dishes to avoid bacterial suspension evaporation due to the air-cooling. The material of the petri dishes does not cut the used light.

The adhesion of the *E. coli* on the TiO$_2$-NTs and Ag/TiO$_2$-NTs anodized surfaces was carried out by immersing the samples into 5 mL suspension of *E. coli* cell of a concentration of 4 10^6 CFU/ml. The tube was then shacked gently at 37°C for 4 h in dark [22,23]. The non-adhered bacteria to the NTs were removed by washing the surface with phosphate buffer solution (pH 7.2). The number of viable cells was determined after detachment of the adhered *E. coli* cells by ultra-sonication (50 W) for 15 min. Non-adhered/weakly adhered bacteria on the surfaces were evaluated according to Hoffman [24]. Bacterial adhesion experiments were carried out in the dark to avoid the photocatalytic action of the TiO$_2$ and Ag/TiO$_2$ surfaces.

2-3. Characterizations

The crystallinity and phase identification of the prepared samples were systematically investigated using X-ray diffraction (Philips X'PERT MPD, Cu Kα irradiation, λ=1.5406Å). The diffraction data were collected over the diffraction angle range of 20°–80° with a scanning step of 0.016°. The morphology and nanostructure of the Ag-NPs/TiO$_2$-NTs samples were examined by scanning electronic microscope (SEM, Jeol JSM-6300) and FEI Tecnai *G*2 transmission electron microscopy (TEM) operating at 200 kV with a LaB6 filament. The local chemical analysis was performed using the energy dispersive X-ray spectroscopy (EDXS) system attached to the TEM. The photoluminescence (PL) measurements on the Ag-NPs/TiO$_2$-NTs samples were carried out by using a fluorescence spectrophotometer (Perkin Elmer LS55) equipped with a xenon lamp at an excitation wavelength of λ = 340 nm. The XPS measurements were performed using an AXIS NOVA (Kratos Analytical, Manchester, UK) photoelectron spectrometer with an achromatic Al Kα X-ray source at 400 W. The spectra were excited using Al Kα radiation (1486.6 eV). All XPS data were corrected from sample charging during XPS data acquisition, while using the C1s (284.6 eV) peak as a reference. The base pressure below 5 10^{-9} mbar was maintained during the

measurement. No argon sputtering was considered as to clean the coatings surface, neither ion or electron neutralizers were used during the measurement. The surface atomic concentration percentage for each element was determined from peak areas using the known sensitivity factors for each element [25,26] on the surfaces. The spectrum background was subtracted according to Shirley [27] through the Shirley subtraction GL(30) program of the Kratos unit. The XPS spectra for the Ti and Ag-species were analyzed using CasaX-Vision 2 (Kratos Analytical, UK) and the peaks were assigned according to the NIST database. All measurements were done in the fixed analyzer transmission mode (FAT).

3. RESULTS AND DISCUSSIONS

X-ray diffraction (XRD) performed on the films showed Bragg reflections between 20 and 80°. Figure 1 shows the XRD spectra of the Ag-NPs/TiO$_2$-NTs, which confirm that all samples, are crystallized in the anatase phase. The extra peaks observed at $2\theta = 38.5°$, $40.4°$, $53.1°$, $63°$, $70.8°$ are due to the Ti metallic phase of the underlying substrate. The absence of silver related XRD peaks is mainly related to the very tiny amount of Ag NPs deposited on the TiO$_2$–NTs. Ag/TiO$_2$ material have been extensively studied. Table 1 shows the diameter of TiO$_2$-NTs expressed as mean value (± standard deviation) and the number of counted particles/NTs for the statistical analysis both for Ag-NPs and for TiO$_2$-NTs. Crystallite size of TiO$_2$-NTs are also estimated by the mean of XRD Scherrer equation as previously reported in detail [21]. Page et al., reported on Silver-titania nanocomposite as potent antimicrobial material and reported XRD peaks assigned to Ag$_2$O at $2\theta=31.5°$ [28]. For our composite, this peak was not observed. This can be attributed to the few amounts of Ag that are likely below the XRD sensitivity threshold. It is readily seen that even at low anodization potentials, Ti crystallizes in anatase phase. This is due to the annealing step for 3 hours at 400°C as described in the experimental section. Recently, Mateus et al., observed anatase phase in TiO$_2$ nanotubes prepared by different chemical solutions/precursors such as water/fluorhydric acid/ammonium fluoride/ethylene glycol (H$_2$O/HF/NH$_4$F/EG) as well as the conditions of anodization. The same authors showed by the mean of UV–Vis measurements that the band-gap varied with to the anodizing time and solution [29].

Figure 2 Shows SEM top view images of Ag NPs decorated TiO$_2$-NTs anodized respectively under potential 20 V (a) and 60 V (b). No tubular structures were seen when applying 20 V. At lower potentials, the fields assisted dissolution was not strong enough to remove the first anodic

layer formed at the beginning of the anodization and leading to the formation of NTs. Under 30 V, the NTs were not clearly seen. However, under 60 V anodization, a highly ordered TiO_2 NTs, vertically aligned onto the Ti-substrate were formed as seen in Figure 2b. Figure 2c shows the diameter size distribution of TiO_2 NTs anodized at 60 V with a mean diameter size of 97 nm. Figure 3d shows the evolution of mean diameter of TiO_2-NTs as function of the applied anodization potentials. A maximum diameter size of 100 nm was reached for an anodization potential of 70 V.

The size distribution of Ag NPs was carried out using TEM on the Ag NPs decorated TiO_2-NTs sample anodized at 60 V. Figure 3a (and the inset) shows a bare TiO_2-NTs with typical outer diameter of 100 nm that confirm the SEM observation. The as-formed TiO_2-NTs are seen in Figure 3b to be highly ordered and vertically aligned onto the underlying Ti-substrate. The observed nanotubes is 100 nm present a length is of ~15 μm (see the SEM cross-section view in the inset of Figure 3b). Figure 3c shows the TiO_2-NTs after their Ag NPs decoration, the Ag NPs are attached on the external wall of the tube. In order to find the average size of Ag-NPs. It is normally difficult to efficiently deposit Ag-NPs in TiO_2 nanotubes using the photo-reduction method. The TEM image were systematically analyzed as shown in Figure 3. The average size of Ag NPs decorating the TiO_2-NTs is about 8 +/-2 nm.

Figure 4 shows the diffuse reflectance spectra of the anodized NTs. It is readily seen from Figure 4 that the spectral absorption of Ag-decorated samples are shifted to the visible region. The yellow zone of the figure shows the light emission of the used light source (solar simulated light, 310-800 nm). The UV-Vis absorbance spectra show that the absorption edges was bleu shifted with the increase of the NTs diameter, which can be explained by the increase of the crystallites average size. Although TiO_2 is an indirect semiconductor and its energy gap is usually estimated by reflectance spectra, the difficulty to get accurate data (band-gaps) from DRS spectra in our case comes from the baseline/background correction before spectra acquisition. After anodization the substrate shows little colorization that is different from the raw material. This colorization limits to a large extend the possibility of using "non-anodized" material as baseline/background. Band-gaps (and intra-gap states) of the prepared NTs are described below by the mean of PL.

Figure 5 shows the typical PL spectra of TiO_2-NTs and Ag decorated TiO_2-NTs anodized at different potentials. When exited with UV light (see experimental) nano-crystalline TiO_2 reveals a range of intra-bandgap defect states that emit at visible wavelengths as shown in the PL spectra.

To probe the luminescent defect states of the anodized TiO_2-NTs shown in this study, we used 340 nm excitation. The TiO_2-NTs show a broad photo-luminescence in the visible (from 380 to 660 nm) with a mono-modal peak at 390-450 nm or 2.7-3.1 eV. The PL spectra of Ag/TiO_2-NTs show bimodal peaks. The first peak (390-450 nm) corresponds to TiO_2-NTs; however, the second peak corresponds to the signal generated by Ag-NPs. This latter peak ranges from 460-650 nm corresponding to band energies 1.9-2.6 eV. The NTs defects were investigated through the shape and shifts in the intensity of the PL spectra correlated to electron/hole pairs and band-gap energies [30,31]. The increase of the photoluminescence (PL) intensity of Ag/TiO_2-NTs indicates the increase of the specific area when the nanotubes diameter increases. Figure 5b shows the bacterial inactivation mechanism on Ag-decorated TiO_2-NTs. Ag NPs increase the separation of photogenerated charges and help in transferring the trapped electrons to the adsorbed O_2. The Fermi level of Ag NPs is situated below the TiO_2 conduction band. This promotes the interfacial charge transfer (IFCT) from TiO_2-NTs to Ag-NPs [30] reducing consequently the charge recombination in TiO_2.

XPS results showed the existence of Ti^{4+} and Ti^{3+} in the as-prepared samples. TiO_2-NTs showed 89% Ti^{4+} and 10% Ti^{3+} as determined by XPS-peaks surface areas. Ag/TiO_2-NTs showed slightly different proportions of 81% and 19%, respectively for Ti^{4+} and Ti^{3+}. Before their use for the antibacterial activity tests, the samples undergo the autoclaving step. After autoclaving, the samples showed slightly different surface properties (oxidative states) as detected by XPS. After autoclaving, the Ti^{3+} content reached 22% for TiO_2-NTs samples and up to 29% for Ag/TiO_2-NTs samples. These changes in the oxidative states can be attributed to the molecular disorders at the NTs interface after autoclaving (H_2O_{vapor} and pressure). After the bacterial inactivation time under light irradiation, the surface oxidative states were also followed. The Ti^{3+} was seen to increase in all samples to 33 to 41% respectively for TiO_2-NTs and Ag/TiO_2-NTs. Ti-oxidative states (Ti^{+3} and Ti^{+4}) have been reported to change between the as-prepared sample and the illuminated sample during the bacterial inactivation [32,33]. At these valences (+3 and +4), the ionic radii are located between 0.65 and 0.88 Å. In addition, Ag species used to decorate the TiO_2-NTs exhibit oxidative states of +1 and +2. The ionic radii of these Ag-species were calculated to be 0.67-1.28 Å and 0.79-0.94 Å for Ag^+ and Ag^{2+}, respectively [34]. Ahrens previously calculated these radii from bond length - bond strength equations [35]. The mechanism of bacterial inactivation on Ag/TiO_2-NTs was reported in many studies before and will not be discussed in deep details in the present work.

Nonetheless, it is worth mentioning that this bacterial inactivation involves IFCT processes occurring between AgO/Ag_2O and TiO_2 [36-38].

Figure 6 shows *E. coli* inactivation on TiO_2-NTs and Ag decorated TiO_2-NTs under low intensity solar simulated light. The used light dose corresponds to the daylight dose during a cloudy day. It is readily seen in Figure 6 that TiO_2-NTs by themselves reduced 1.6log *E coli* within 180 min. Ag decorated TiO_2-NTs enhanced the bacterial inactivation. The fastest bacterial inactivation was seen to happen on Ag/TiO_2-NTs anodized at 60 V and 70 V inactivating 99.99% *E. coli* within 90 min. It has been reported recently that bacteria can adhere to nanostructured TiO_2 based surfaces due to Lifshitz-Van der Waals forces, hydrogen bonding, electrostatic interactions and Brownian motion interfacial forces [39,40]. This adhesion was also attributed to the cell wall proteins interaction with the surface [41] and the surface wettability at the solid-liquid interface [42]. *E. coli* adhesion on the TiO_2-NTs and Ag/TiO_2-NTs in the dark showed that increasing the incubation time of bacteria with the surface increases the bacterial adhesion until a certain limit of $\sim10^3$ $CFU/ml/cm^2$. This load is weak compared to other surfaces able to harbor higher bacterial concentrations. This is due to: i) bacterial cell wall interaction with the polar groups on the NTs-surface, ii) the wetting property of the NTs-surface (decorated with Ag or not), and iii) the surface potential "*Eigenvalues*" as recently reported [7]. It has been recently reported that the cell wall complexity controls the adhesion and invasion of biotic and abiotic surfaces [43]. Figure 6 shows that *E. coli* can adhere to TiO_2-NTs in the dark. Under light, this bacterial adhesion facilitates the charge transfer between the photocatalyst and the bacterial cell wall leading to cell wall damage [44]. The TiO_2 photo-switchable surface wettability was extensively reported in the literature [45,46] and is beyond the scope of the present study focusing more on the effect of the NTs geometry on the bacterial inactivation. Figure 6 shows also a slight bacterial inactivation in the dark on Ag/TiO_2-NTs. This can be due to the diffusion of Ag-ions to the bacterial cytoplasm through the cell wall porins.

In addition, Figure 3d showed that the size distribution of Ag-NPs ranges from 1 to 12 nm. Nowack et al., [47] reviewed the use of nano-silver and the associated antibacterial effect during the last decades. Rtimi et al., reported that the dissolution of Ag-NPs releasing Ag-ions and attributed the antibacterial activity to an oligodynamic effect [48,14]. These ions are able to penetrate the bacterial cell envelop, reaching the cytoplasm and inactivating the cell machinery and

thus leading to cell death. Recent reports used porinless bacteria to not allow the penetration of Ag-ions through the bacterial cell wall porins [49,50]. The same study showed that porinless *E. coli* inactivation was six times longer than normal/wild *E. coli* (with porins). This study gave the evidence that Ag-ions are not the only agent leading to the bacterial inactivation but that surface-contact effects play also an important role through ROS and/or charge transfer [49-51]. *E. coli* has a thinner peptidoglycan cell wall compared to the *S. aureus* and containing additional layers with a high structural complexity. The significant difference in the cell wall thickness/microstructure between these strains may lead to different interactions with TiO_2-NTs and Ag/TiO_2-NTs surfaces. TiO_2 was reported to damage the cell wall membrane through lipid-peroxidation [51] increasing the cell wall fluidity [32]. Nesic et al., reported recently on bacterial inactivation on TiO_2 impregnated textiles in the dark [9, 33].

CONCLUSION

TiO_2-NTs have been successfully prepared from the anodization of metallic Ti foils, and decorated them with Ag-NPs using the photochemical reduction method. By varying the anodization potential, we were able to increase the nanotubes diameter until reaching 100 nm for 70V. The increase of the anodization potential led to an increase in the crystallites sizes. It was also seen that PL spectra revealed band-gaps in the range of 2.7-3.1 eV for TiO_2 and of 1.9-2.5 for Ag_xO. The reduced surface defects of TiO_2 where seen to enhance the photocatalytic bacterial inactivation kinetics. The maximum photocatalytic performance of TiO_2-NTs is obtained for NTs anodized at 60 and 70V. Bacterial adhesion was seen to be favorable in the dark. Under light irradiation, the bacterial inactivation was seen to be faster on larger NTs prepared at 60-70 V. The Ag/TiO_2-NTs reported in this study have the potential to open new industrial segments in the rapidly developing health sector. Further research is required to translate the present findings into performing industrial products e.g. medical devices and implants.

REFERENCES

[1] E. A. Zottola and L. B. Smith, The microbiology of foodborne disease outbreaks: an update, J. Food Safe 11 (1990) 13-29.

[2] K. Gopal, S. S. Tripathy, J. L. Bersillon, S. P. Dubey, Chlorination byproducts, their toxicodynamics and removal from drinking water, *J. Hazard. Mater.* 140 (2007) 1-6.

[3] J. L.Graves Jr, M. Tajkarimi, Q. Cunningham, A. Campbell, H. Nonga, S. H. Harrison, J.E. Barrick, Rapid evolution of silver nanoparticle resistance in *Escherichia coli*, Frontier in Genetics 6 (2015) Article 42.

[4] V. Tangcharoensathien, S. Chanvatik, A. Sommanustweechai, Complex determinants of inappropriate use of antibiotics, Bull World Health Organ 96 (2018) 141–144.

[5] S. Rtimi, Indoor Light Enhanced Photocatalytic Ultra-Thin Films on Flexible Non-Heat Resistant Substrates Reducing Bacterial Infection Risks, Catalysts 7 (2017) 57.

[6] M.K.S. Ballo, S. Rtimi, J. Kiwi, C. Pulgarin, J.M. Entenza, A. Bizzini, Fungicidal activity of copper-sputtered flexible surfaces under dark and actinic light against azole-resistant *Candida albicans* and *Candida glabrata*, *Journal of Photochemistry & Photobiology, B: Biology* 174 (2017) 229-234.

[7] A. Camarasa Mena, S. Rtimi, C. Pulgarin, J-C Lavanchy, J. Kiwi, Grafted semiconductors on PE-films leading to bacterial inactivation: synthesis, characterization and mechanism, *Colloids and Surfaces A: Physicochemical and Engineering Aspects* 519 (2017) 231-237.

[8] P. Ganguly, C. Byrne, A. Breen, S. C. Pillai, Antimicrobial activity of photocatalysts: Fundamentals, mechanisms, kinetics and recent advances, Applied Catalysis B: Environmental 225 (2018) 51-75.

[9] J. Nesic, S. Rtimi, D. Laub, G. M. Roglic, C. Pulgarin, J. Kiwi, New evidence for TiO_2 uniform surfaces leading to complete bacterial reduction in the dark: Critical issues, *Colloids and Surfaces B: Biointerfaces*, 123 (2014) 593-599.

[10] F. Petronella, S. Rtimi, R. Comparelli, R. Sanjines, C. Pulgarin, M. L. Curri, J. Kiwi, Uniform TiO_2/In_2O_3 surface films effective in bacterial inactivation under visible light, Journal of Photochemistry and Photobiology A: Chemistry 279 (2014) 1-7.

[11] Bin Guo, Elodie V. Pasco, Irene Xagoraraki, Volodymyr V. Tarabara, Virus removal and inactivation in a hybrid microfiltration–UV process with a photocatalytic membrane, Separation and Purification Technology 149 (2015) 245–254.

[12] Horst Kisch, Semiconductor Photocatalysis-Mechanistic and Synthetic Aspects, Angew. Chem. Int. Ed. 52 (2013) 812-847.

[13] I. Milosevic, A. Jayaprakash, B. Greenwood, B. van Driel, S. Rtimi, P. Bowen, Synergistic Effect of Fluorinated and N Doped TiO_2 Nanoparticles Leading to Different Microstructure and Enhanced Photocatalytic Bacterial Inactivation, Nanomaterials 7 (2017) 391.

[14] S. Rtimi, R. Sanjines, C. Pulgarin, A. Houas, J.-C. Lavanchy, J. Kiwi, Coupling of narrow and wide band-gap semiconductors on uniform films active in bacterial disinfection under low intensity visible light: Implications of the interfacial charge transfer (IFCT), Journal of Hazardous Materials 260 (2013) 860-868.

[15] A. Pearson, H. Zheng, K. Kalantar-zadeh, S. K. Bhargava, V. Bansal, Decoration of TiO_2 Nanotubes with Metal Nanoparticles Using Polyoxometalate as a UV-Switchable Reducing Agent for Enhanced Visible and Solar Light Photocatalysis, Langmuir 28 (2012) 14470-14475.

[16] A. Fujishima, X. Zhang, D. Tryk, TiO_2 Photocatalysis and Related Surface Phenomena. Surf. Sci. Rep. 2008, 63, 515–582.

[17] M. Landmann, E. Rauls, W. G. Schmidt, The Electronic Structure and Optical Response of Rutile, Anatase and Brookite TiO_2. J. Phys. Condens. Matter 2012, 24, 195503.

[18] J. Zhang, P. Zhou, J. Liu, J. Yu, New Understanding of the Difference of Photocatalytic Activity among Anatase, Rutile and Brookite TiO_2. Phys. Chem. Chem. Phys. 2014, 16, 20382–20386.

[19] A. Testino, I. R. Bellobono, V. Buscaglia, C. Canevali, M. D'Arienzo, S. Polizzi, R. Scotti, F. Morazzoni, Optimizing the Photocatalytic Properties of Hydrothermal TiO2 by the Control of Phase Composition and Particle Morphology. A Systematic Approach, J. AM. CHEM. SOC. 129 (2007) 3564-3575.

[20] T. Zhang, X. Hu, M. Fang, L. Zhang, Z. Wang, Synthesis of hierarchical TiO_2 nanotube arrays assembled by anatase single crystal nanoparticles, CrystEngComm. 14 (2012) 7656-7661.

[21] M. Mangayayam, J. Kiwi, S. Giannakis, C. Pulgarin, I. Zivkovic, A. Magrez, S. Rtimi, FeOx magnetization enhancing *E. coli* inactivation by orders of magnitude on Ag-TiO_2 nanotubes under sunlight, *Applied Catalysis B: Environmental* 202 (2017) 438–445.

[22] A. Bonnefond, E. González, J. M. Asua, J. R. Leiza, J. Kiwi, C. Pulgarin, S. Rtimi, New evidence for hybrid acrylic/TiO_2 films inducing bacterial inactivation under low intensity simulated sunlight, Colloids and Surfaces B: Biointerfaces 135 (2015) 1-7.

[23] O. Seddiki, C. Harnagea, I. Levesque, D. Mantovani, F. Rosei, Evidence ofantibacterial activity on titanium surfaces through nanotextures, Appl. Surf.Sci. 308 (2014) 275-284.

[24] R. Kadlec, M. Jakubec, Z. Jaglic, A novel flotation technique for the separation of non-adherent microorganisms from a substrate, Lett. Appl. Microbiol. 58(2014) 604–609.

[25] Wagner, C.D.; Riggs, M.W.; Davis, E.L.; Müllenberg, E.G. (Eds) Handbook of X-Ray Photoelectron Spectroscopy, Perkin-Elmer Corp. Phys. Electronic Division, 1979.

[26] J.C. Rivière and S. Myhra, Handbook of Surface and Interface Analysis: Methods for Problem-Solving, 2nd Edition, CRC Press (Taylor & FrancisGroup), UK 2009, 32-64.

[27] D.A. Shirley, High-Resolution X-Ray photoemission spectrum of the valence bands of gold, Phys. Revs. B5 (1972) 4709-4714.

[28] K. Page, R. G. Palgrave, I. P. Parkin, M. Wilson, S. L. P. Savin and A. V. Chadwick, Titania and silver-titania composite films on glass - potent antimicrobial coatings, J. Mater. Chem. 17 (2007) 95-104.

[29] H. M. Mateus, J. Barba‑Ortega, M. R. Joya, Comparison of the Growth of TiO_2 Nanotubes in Different Solutions, J. Inorg. Organomet. Pol. Mats. 28 (2018) 612-623.

[30] N. Pugazhenthiran, S. Murugesan, S. Anandan, High surface area Ag-TiO_2 nanotubes for solar/visible-light photocatalytic degradation of ceftiofur sodium, J. Haz. Mat. 263 (2013) 541-549.

[31] Shusheng Pan, Xiaolin Liu, Min Guo, Siu fung Yu, Haitao Huang, Hongtao Fan and Guanghai Li, Engineering the intermediate band states in amorphous Ti^{3+}-doped TiO_2 for hybrid dyesensitized solar cell applications, J. Mat. Chem. A 3 (2015) 11437.

[32] S. Rtimi, R. Sanjines, M. Andrzejczuk, C. Pulgarin, A. Kulik, J. Kiwi, Innovative transparent non-scattering TiO_2 bactericide thin films inducing increased *E. coli* cell wall fluidity, Surface & Coatings Technology 254 (2014) 333–343.

[33] S. Rtimi, J. Nesic, C. Pulgarin, R. Sanjines, M. Bensimon and J. Kiwi, Effect of surface pretreatment of TiO_2 films on interfacial processes leading to bacterial inactivation in the dark and under light irradiation, Interface Focus 5 (2015) 20140046.

[34] "Revised Effective Ionic Radii and Systematic Studies of Interatomic Distances in Halides and Chalcogenides" By R. D. Shannon. Central Research and Development Department, Experimental Station, E. I. Du Pont de Nemours and Company, Wilmington, Delaware 19898, U.S.A.

[35] L. H. Ahrens, The use of ionization potentials Part 1. Ionic radii of the elements, Geochim. Cosmochim. Acta 2 (1952) 155-169.

[36] K. Ubonchonlakate, L. Sikong, F. Saito, Photocatalytic disinfection of *P.aeruginosa* bacterial Ag-doped TiO_2 film, Procedia Engineering 32 (2012) 656-662.

[37] S. Rtimi, O. Baghriche, R. Sanjines, C. Pulgarin, M. Bensimon, J. Kiwi, TiON and TiON-Ag sputtered surfaces leading to bacterial inactivation under indoor actinic light, *J. Photochemistry and Photobiology A: Chemistry*, 256 (2013) 52-63.

[38] J. Prakash, S. Sun, H. C. Swart, R. K. Gupta, Noble metals-TiO_2 nanocomposites: From fundamental mechanisms to photocatalysis, surface enhanced Raman scattering and antibacterial applications, Applied Materials Today 11 (2018) 82-135.

[39] H. J. Busscher, H. C. van der Mei, How Do Bacteria Know They Are on a Surface and Regulate Their Response to an Adhering State? PLoS Pathogens 8 (2012) e1002440.

[40] H. H. Tuson and D. B. Weibel, Bacteria-surface interactions, Soft Matter. 9 (2013) 4368-4380.

[41] M. Rabe, D. Verdes, S. Seeger, Understanding protein adsorption phenomena at solid surfaces, Advances in Colloid and Interface Science 162 (2011) 87-106.

[42] M. Kastantin, B. B. Langdon, D. K. Schwartz, A bottom-up approach to understanding protein layer formation at solid–liquid interfaces, Advances in Colloid and Interface Science 207 (2014) 240-252.

[43] F. Lamari, I. Chakroun, S. Rtimi, Assessment of the correlation among antibiotic resistance, adherence to abiotic and biotic surfaces, invasion and cytotoxicity of Pseudomonas aeruginosa isolated from diseased gilthead sea bream, Colloids and Surfaces B: Biointerfaces 158 (2017) 229-236.

[44] O. Baghriche, S. Rtimi, C. Pulgarin, C. Roussel, J. Kiwi, RF-plasma pretreatment of surfaces leading to TiO_2 coatings with improved optical absorption and OH-radical production, Applied Catalysis B: Environmental 130-131 (2013) 65-72.

[45] S. Rtimi, C. Pulgarin, R. Sanjines and J. Kiwi, Innovative semi-transparent nanocomposite films presenting photo-switchable behavior and leading to a reduction of the risk of infection under sunlight, RSC Adv. 3 (2013) 16345-16348.

[46] I. Ahmad and C.-W. Kan, Visible-Light-Driven, Dye-Sensitized TiO_2 Photo-Catalyst for Self-Cleaning Cotton Fabrics, Coatings 7 (2017) 192.

[47] B. Nowack, H. F. Krug, and M. Height, 120 Years of Nanosilver History: Implications for Policy Makers, Environ. Sci. Technol. 45 (2011) 1177-1183.

[48] S. Rtimi, M. Pascu, R. Sanjines, C. Pulgarin, M. Ben-Simone, A. Houasa, J.-C. Lavanchy, J. Kiwi, ZrNO-Ag co-sputtered surfaces leading to *E. coli* inactivation under actinic light: Evidence for the oligodynamic effect, J. Haz. Mat. 260 (2013) 860-868.

[49] S. Rtimi, V. Nadtochenko, I. Khmel and J. Kiwi, Evidence for differentiated ionic and surface contact effects driving bacterial inactivation by way of genetically modified bacteria, Chem. Comm. 53 (2017) 9093.

[50] S. Rtimi, V. Nadtochenko, I. Khmel, M. Bensimon and J. Kiwi, First unambiguous evidence for distinct ionic and surface-contact effects during photocatalytic bacterial inactivation on Cu–Ag films: Kinetics, mechanism and energetics, *Mat. Tod. Chem.* 6 (2017) 62-74.

[51] C. Ruales-Lonfat, N. Benitez, A. Sienkiewicz, C. Pulgarin, Deleterious effect of homogeneous and heterogeneous near-neutral photo-Fenton system on *Escherichia coli*. Comparison with photo-catalytic action of TiO_2 during cell envelope disruption, Applied Catalysis B: Environmental 160-161 (2014) 286-297.
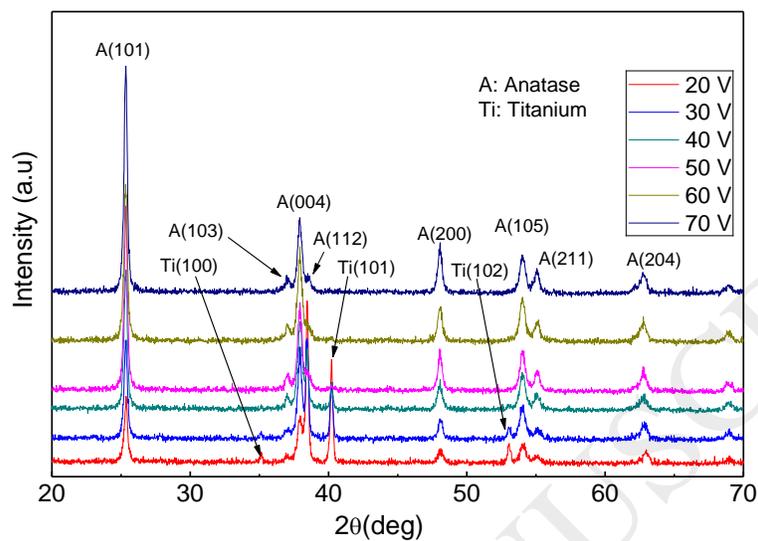
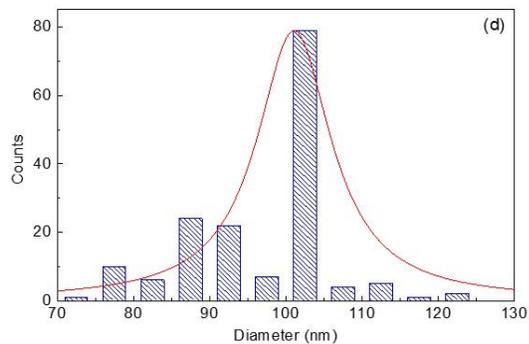**Figure 1.** XRD patterns of Ag-NPs decorated TiO$_2$-NTs as a function of anodization potential.
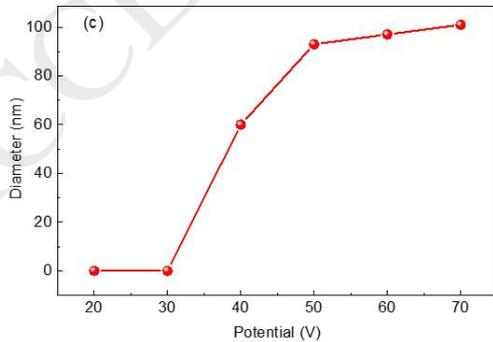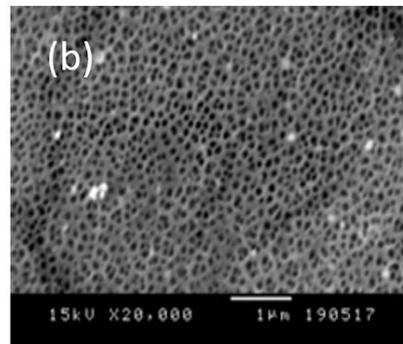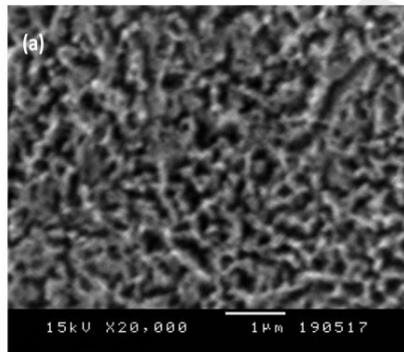
Figure 2. SEM top view images of Ag-NPs decorated TiO_2-NTs anodized respectively under : (a) potential 20 V, and (b) 60 V. (c) the variation of diameter of the TiO_2-NTs as function of anodization potentials, and (d) the diameter size distribution of TiO_2-NTs anodized at 60 V.
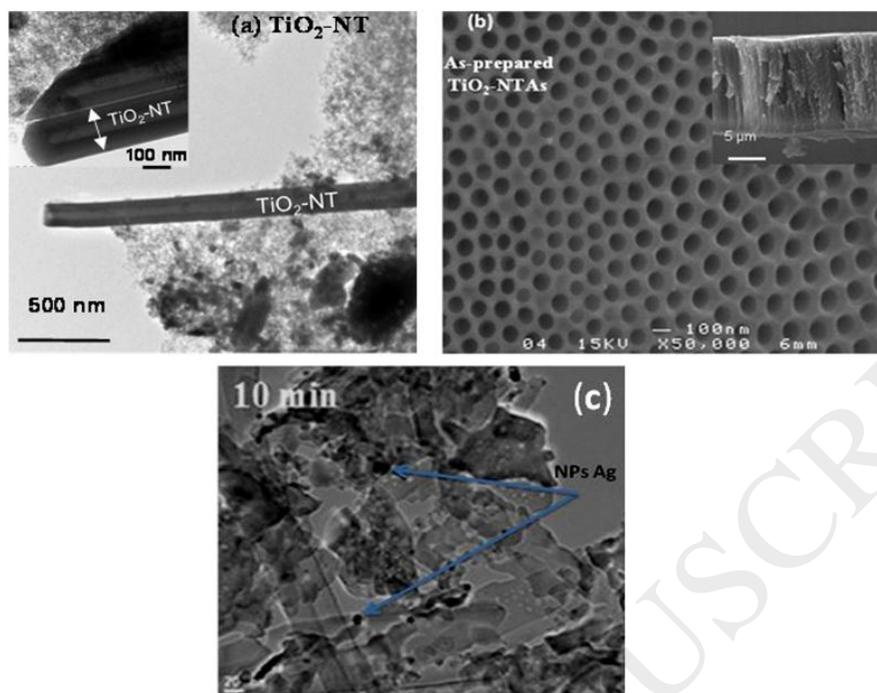
Figure 3. Typical TEM micrographs of an undecorated TiO$_2$-NT (a) and a TiO$_2$-NT decorated with Ag-NPs during 10 min of photo-reduction time (b), SEM top-view image of the prepared TiO$_2$-NTs (60 V), and (c) TEM of Ag-NPs prepared by photo-reduction method for 10 min.
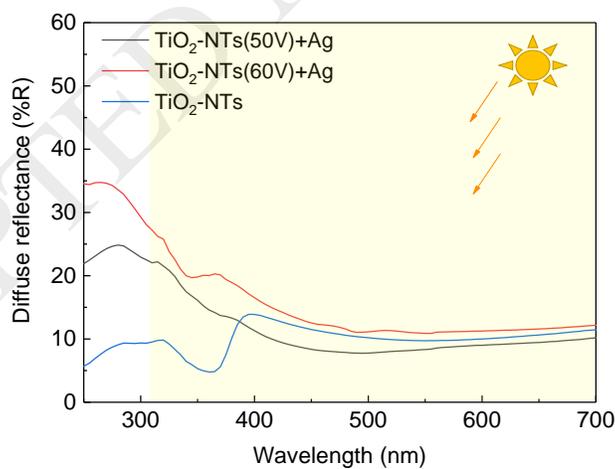

Figure 4. Diffuse reflectivity spectra of TiO$_2$-NTs decorated with Ag-NPs grown at different anodization potential. The yellow zone in the figure represents the emission range of the applied light (310-800 nm).
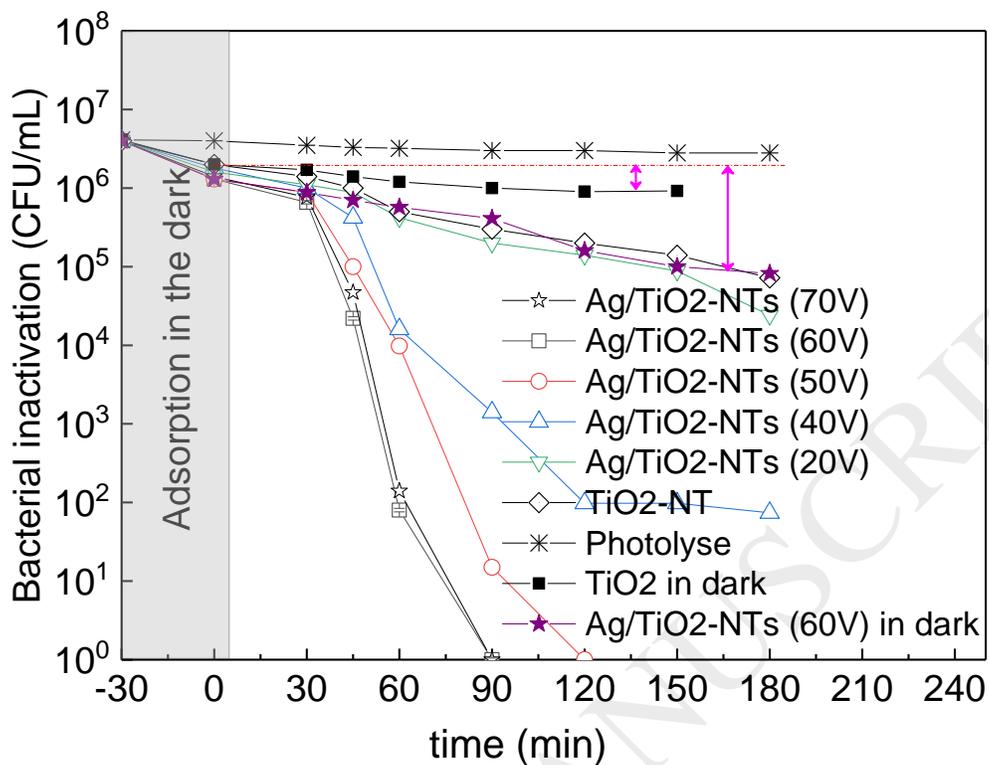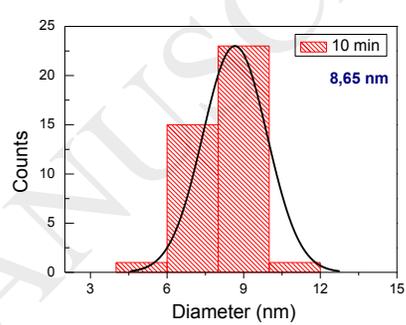
Figure 5. a) Typical PL spectra of Ag-NPs decorated TiO$_2$-NTs anodized at different potential; b) mechanism of bacterial inactivation on Ag decorated TiO$_2$-NTs.

Figure 6. Bacterial inactivation on TiO$_2$-Nts and TiO$_2$-NTs+Ag. Used light: solar simulated light (50 mW/cm^2, 310-800 nm). For more details, see text. (Error bars: SD, n=5%).

Table 1: TiO$_2$-NTs diameter and Ag-NPs size expressed as mean value (± standard deviation).

Anodization potential (V)	Number of nanotubes counted (N)	Mean diameter (nm)	Standard deviation (SD)	Crystallites size (nm)
20	No NT formed yet*	-	-	31 ± 1.5
30	No NT formed yet*	-	-	29.4 ± 1.8
40	41	59.6	13.702	29.4 ± 1.8
50	131	93.6	9.27	31.7 ± 2.1
60	161	96.6	9.25	27.9 ± 1.8
70	155	100.9	15.48	29.2 ± 1.9

Ag NPs size distribution

Mean diameter: (nm)	8.65	
SD:	1.26	
Particles number counted:	40	

*: Please see supplementary figure 1 for the microscopy images and NTs formation at different anodization voltages.